Steel and Composite Structures, *Vol. 28, No. 6 (2018) 767-778*
DOI: https://doi.org/10.12989/scs.2018.28.6.767

Effect of bolted splice within the plastic hinge zone on beam-to-column connection behavior

Cüneyt Vatansever* and Kutay Kutsal

Department of Civil Engineering, Istanbul Technical University, 34469, Maslak, Istanbul, Turkey

(*Received November 23, 2017, Revised August 9, 2018, Accepted September 3, 2018*)

Abstract. The purpose of this study is to investigate how a fully restrained bolted beam splice affects the connection behavior as a column-tree connection in steel special moment frames under cyclic loading when located within the plastic hinge zone. The impacts of this attachment in protected zone are observed by using nonlinear finite element analyses. This type of splice connection is designed as slip-critical connection and thereby, the possible effects of slippage of the bolts due to a possible loss of pretension in the bolts are also investigated. The 3D models with solid elements that have been developed includes three types of connections which are the connection having fully restrained beam splice located in the plastic hinge location, the connection having fully restrained beam splice located out of the plastic hinge and the connection without beam splice. All connection models satisfied the requirement for the special moment frame connections providing sufficient flexural resistance, determined at column face stated in AISC 341-16. In the connection model having fully restrained beam splice located in the plastic hinge, due to the pretension loss in the bolts, the friction force on the contact surfaces is exceeded, resulting in a relative slip. The reduction in the energy dissipation capacity of the connection is observed to be insignificant. The possibility of the crack occurrence around the bolt holes closest to the column face is found to be higher for the splice connection within the protected zone.

Keywords: steel moment frames; steel beam-to-column connections; column-tree connection; beam splice; plastic hinge; protected zone; finite element analysis; plastic equivalent strain; rupture index

1. Introduction

Steel moment resisting frames are one of the lateral load resisting systems, which could be used with steel braced frames and steel plate shear walls, depending on the architecture and height of the structure. The types of steel moment resisting frames are determined according to the level of seismicity in the regions that the structures are going to be constructed. While ordinary and intermediate moment frames are used in the regions having a low seismic risk, with the increasing probability of the severe earthquake special moment frames are preferred in high seismic zone. When a building with steel moment resisting frames to be built in high seismic zone are designed, several requirements, which are indicated in specifications, shall be satisfied to obtain frames that are more ductile under severe ground motion. When ductile steel moment frames are designed, it is aimed to concentrate the large plastic deformations in the plastic hinge region, which is intended to occur in beams, and to keep the high plastic deformation away from the column so that the structure could exhibit superior performance in earthquakes.

After the gained experience from the severe earthquakes, many engineers started to study on improving the connection as doing lots of research and experiment. Others preferred to choose different lateral load resisting systems and to use column-tree connection which is recently one of the connections commonly used in USA, Korea and Japan (Astaneh 1997).

Shop-fabricated column-tree connections consist of two beam parts which are link beam and stub beam. First, the stub beam is welded to column in the shop, and then the column-tree is erected in the field. After erection is achieved, link beam is spliced to the stub beam with high strength bolts. Since the connection between the stub beam and the column are provided in the shop, quality control of welding process can be carried out easily. In contrast to that, the cost of welding process is high and the inspection of the weld is usually hard in the case of use of field-welded connection (Oh *et al*. 2014). For this reason, considering the importance of beam-to-column joint where it is expected to dissipate large amount of energy during severe seismic motion, preferring column-tree connection in special moment frames have various advantages in terms of cost-effectiveness and weld quality.

Numerous experimental studies were carried out on column-tree connections, containing different types of parameters that directly affect the behavior of the beam-to-column joints. Oh *et al*. (2014) have investigated the cyclic behavior of the column-tree connection which includes weakened beam splice. The reference point in this study is that if the beam splice is located at a certain distance away from the column face, there is no need that the plastic

*Corresponding author, Ph.D., Assistant Professor, E-mail: cuneyt.vatansever@itu.edu.tr
[a] Ph.D. Student, E-mail: kutsal@itu.edu.tr

ISSN: 1229-9367 (Print), 1598-6233 (Online)

moment capacity of the beam splice is greater than the plastic moment capacity of the connected beam. The test results have shown that moment resisting capacity of the specimens with weakened beam splices did not decrease clearly. Hence, it was demonstrated that beam splice could be designed with a plastic moment capacity lower than that the connected beam, locating at certain distance away from column face. The use of reduced beam section concept has been also found as a good resource of dissipating energy during cyclic loading. The effects of the beam splice location in the column-tree connection have been investigated by Lee *et al*. (2014a). The results of the study showed that the column tree connection had better bolt slip resistance as the beam splice was moved away from the column face. Lee *et al*. (2014b) have also investigated the cyclic performance of the weak axis column-tree connection, assuming that plastic hinge is formed at beam splice connection. The formation of plastic hinge at the beam splice was provided by reducing the cross-sectional area of the splice plates. The effects of the location of the beam splice were the other parameter studied in this research. Test results showed that reducing the cross-sectional area of the flange splice plates allows the connection to take more advantage of the steel ductility, whereas it could not increase energy dissipation capacity. Oh *et al*. (2015) studied the seismic performance of weak axis column-tree connection commonly used in Korea. In the scope of the study, a reduced beam section and tapered beam section implemented to stub beam in column-tree connection. The result of the experiment showed that the specimen with reduced beam section concept was more ductile and had more energy dissipation capacity than the other specimens. One of the experimental studies regarding the effects of bolt slippage in column-tree connection, having beams with different length-to-height ratio of the beam, carried out by Lee *et al*. (2016). Quasi-static cyclic loading was applied to the specimens having the variable length-to-depth ratio in order to obtain the effects of bolt slippage. As a result of this experimental study, the least bending moment at the column face was obtained from the specimen having the beam with the smaller depth. It was shown that the small value of the length-to-depth ratio, slippage of the bolt did not affect the structural system apparently. Yet, as selecting feasible length-to-depth ratio, bolt slippage could be adjusted in beam-to-column connections in order to ensure that the structure exhibits better seismic performance.

Experimental studies carried out by FEMA/SAC have shown that the regions having high-order plastic deformations are susceptible to discontinuities due to rapid cross-section change and other structural extensions in those regions, and crack initiation may occur in these regions. The expected plastic hinge zone in the connection of steel special moment frames could also be regarded as one of these susceptible zones as it is expected to be subjected to intense plastic deformation during a severe earthquake. These regions are defined as "protected zone" according to AISC 341-16 and AISC 358-16. Any applications in protected zone, that have been done during erection or fabrication, such as tack welds, holes, erection aids, air-arc gouging, and unspecified thermal cutting should be repaired as specified in AISC 341-16. Using of welded, bolted and screwed attachments, shear studs and any application that leads to disturbance of the beam flange also shall not be permitted in this zone in which the large inelastic deformations are concentrated.

The aim of this study is to investigate how a fully restrained bolted beam splice affects the beam-to-column connection behavior in steel special moment frames under seismic loads when located within the plastic hinge zone. The impacts of an attachment in protected zone is also observed with locating fully restrained bolted beam splice in the plastic hinge zone which could be identified as protected zone as per AISC 341-16. Generally, this type of connection consists of slip-critical connection, and it is designed in such a way that the slip between the surface of the splice plates does not occur. In case of the possible loss of pretension in the bolts, the effects of the slippage in the connection located within the zone of the plastic hinge if the friction force between the contact surfaces is exceeded are also investigated.

2. Design of the connection models

Three connection models, shown in Figs. 1(a)-(b)-(c), were developed to determine the effects of fully restrained bolted beam splice when located within plastic hinge on beam-to-column connection behavior. There are two types of connection model having fully restrained bolted splice. While one of which (CIP) is located within plastic hinge zone, the other (COP) is located out of plastic hinge zone. The third one (CWB) is considered without beam splice similar to the Welded Unreinforced Flange-Welded Web Connection as stated in AISC 358-16.

It is assumed that the beam-to-column connections were provided by all-around fillet welded connection. The experimental studies performed by Okazaki *et al*. (2009) shows that the connections having proposed all-around fillet weld with adequate weld size exhibited excellent cyclic performance and had high amount of shear strength, compared with the connections which is formed by using complete joint penetration groove weld. The height of the column was taken as 3.0 m, which corresponds the height between the middle of the two consecutive columns, and the beam length was taken as 3.0 m long.

Column and beam profiles were selected as European hot rolled sections IPE 450 and HD 400×314, respectively with the steel grade of S235. Splice plates used for the connection models having fully restrained bolted beam splice were designed as to have more strength than the connected beam in order to withstand high flexural moment developed within the plastic hinge zone. Thus, S275 steel grade was preferred both flange and web splice plates in the connection. Since no any tensile test was performed for the basic material properties, nominal yield strength and nominal tensile strength of those steel grades, shown in Table 1, were considered in this study.

Since the beam splice connection was considered as slip critical connection, high strength bolts (10.9) were used as

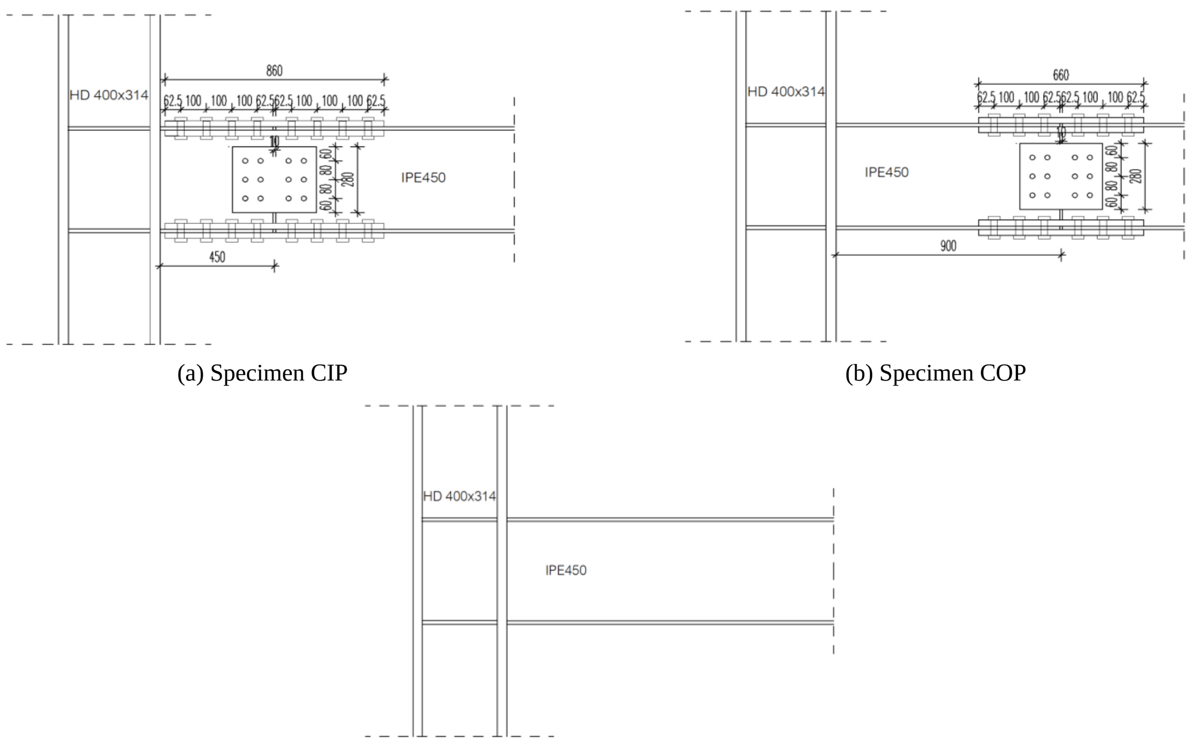

(a) Specimen CIP (b) Specimen COP

(c) Specimen CWB

Fig. 1 Details of the connection models

Table 1 Elements of column-tree connection models

Element	Steel	F_y (MPa)	F_u (MPa)	Elastic modulus (MPa)
IPE 450	S235	235	360	200000
HD 400×314	S235	235	360	200000
Splice plates	S275	275	410	200000
Bolt	10.9	900	1000	200000

stated in AISC 360-16. This specification also states that the limit states that shall be satisfied in the case of preferring slip critical connection shall also be satisfied for bearing type connection. Thus, both slip critical connection and bearing type connection limit states were satisfied in design stage for the connection elements.

Specimen CIP was designed to withstand the expected moment capacity of the connected beams because of the fact that fully restrained bolted splice was located in the expected plastic hinge zone, nearly 450 mm away from the column face, in the beam. Considering this circumstance, twelve number of M27 10.9 high strength bolts were used per one flange splice plate. In contrast to the specimen CIP, thickness of the flange plates and the number of bolts used per flange splice plate were reduced for specimen COP, because the beam splice of this specimen was away 900 mm from the column face, thus kept away from the plastic hinge zone. Table 2 summarizes the properties of splice elements used in the column tree connections, CIP and COP. For the web splice connection twelve number of M20 10.9 high strength bolts were used for both connection models.

The requirements for special moment frames according to AISC 341-16 were also satisfied. Strong column-weak beam condition was satisfied to avoid soft-story mechanism causing collapse of the building with large story drift. It is assumed that lateral bracings were provided every one meter of the beam to prevent out of plane deformation of

Table 2 Column-tree connection models

Specimen	Distance from column face (mm)	Location	Flange splice plates		Web splice plates	
			Type	Bolts	Type	Bolts
CIP	450	Top	860×190×25	32	425×300×10	12
		Bottom	2×860×80×25			
COP	900	Top	660×190×20	24	425×300×10	12
		Bottom	2×660×80×20			

Table 3 Width-to-thickness ratio of elements

Profile	b mm	t_f mm	b / t_f	Limit	h mm	t_w mm	h / t_w	Limit
IPE 450	95	14.6	6.51	7.89	378.8	9.4	40.30	63.37
HD 400×314	200.5	39.8	5.06		289.8	24.9	11.64	

the beam. Since the thickness of panel zone was enough in order to resist shear forces to be developed in that zone, there was no need to reinforce that zone with doubler plate. In order to provide high ductility condition in connection models, another important parameter to be satisfied as per AISC 341-16 was that the beam has appropriate width-to-thickness ratio, and IPE 450 and HD 400×314 profiles were satisfied this requirement, as shown in Table 3.

3. Finite element analysis

3.1 Finite element models (FEMs)

General-purpose finite element analysis software ABAQUS (Hibbit *et al*. 2017) was utilized to simulate all connection models. The connection models include three types of specimens with fully restrained beam splice located in the plastic hinge location (CIP), the specimen with fully restrained beam splice located out of the plastic hinge region (COP) and the connection without beam splice (CWB) as shown in Figs. 2(a)-(b)-(c).

Basically, the solid elements with incompatible modes such as C3D8I can be efficient to capture local instabilities such as flange and/or web buckling without the need to introduce imperfections in the model (Vasdravellis *et al*. 2012). However, initially both C3D8R and C3D8I have separately been tried to verify the FE modelling technique without incorporating the initial imperfection and it has been seen that FE models with solid elements named C3D8R provides more compatible results with those from experimental researches considered for verification. Accordingly, all cross sectional elements of both beam and column were modeled with 8-node linear brick reduced integration elements (C3D8R). Minimum 4 layers of elements were used through the thickness of the parts in the connection models as indicated in Han *et al*. (2016). The fillet welds connecting the stub beam to the column flange were not introduced in the models, because Okazaki *et al*. (2009) reported that excellent cyclic performance was achieved by the specimen having the connection with all-around fillet weld. Furthermore, though adding the welds into the models may affect the analyses results in terms of flexural stiffness of the beam-to-column connection, it is assumed that this effect would be small enough to be neglected in this study.

In order to represent the elastic characteristic of the structural steel elastic modulus and Poisson's ratio were

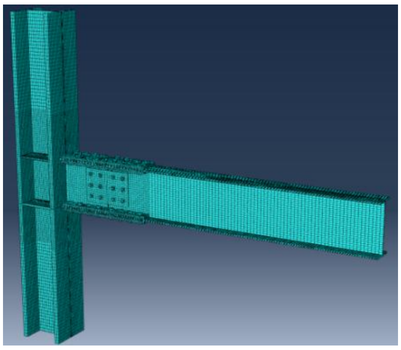

(a) FEM of specimen CIP

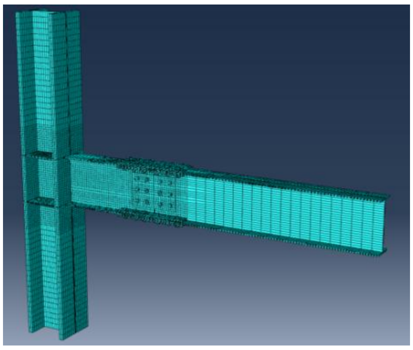

(b) FEM of specimen COP

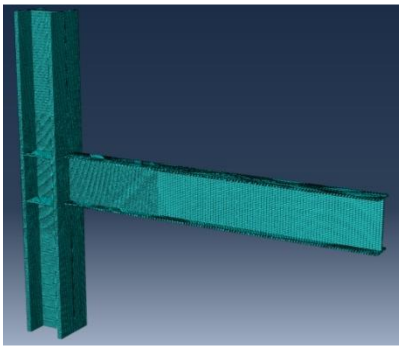

(c) FEM of specimen CWB

Fig. 2 FEM of the connection models

taken as 200000 MPa and 0.3 respectively. Large displacement formulation was utilized to account the geometric nonlinearities in the models. Von Mises yield criterion was preferred so as to define the material nonlinearities. Combined hardening rule, which reflects both characteristics of kinematic and isotropic hardening rules, was considered in the models. Kumar *et al*. (2015) indicated that even if growth of yield surface in the multi-dimensional stress is well-represented by isotropic hardening rule, it does not take into account the reduction in the yield stress known as the Bauschinger Effect. Thus, combined hardening rule may be implemented in the numerical analysis so as to consider the behavior of the structural steel under cyclic loading, considering the loading direction.

Since cyclic coupon test has not been carried out, there was not any available test data for the structural steel subjected to the cyclic loading used in this study. For this reason, the cyclic test data which had been obtained by Kaufmann *et al*. (2001) was employed to consider plasticity model of the structural steel under cyclic loading. The researchers have showed that the stabilized cyclic test data obtained from the tests carried out for different types of steel could be fitted to the Eq. (1), where n is the cyclic strain hardening component. Stress-strain curves were obtained with using the appropriate coefficients of K and n for theevery structural steel used in this study.

$$\sigma = K\varepsilon^{n} \tag{1}$$

Interactions between the contact surfaces of the elements were defined as normal and tangential components. Coulomb friction model was utilized to represent the tangential component, whereas hard contact definition was used to describe the normal behavior of the contact surfaces.

The bottom and top of the column have pin boundary conditions in all connection specimens. In order to avoid out of plane instability, the beam elements were laterally supported at intervals of 1.0 m.

Loading sequences, which are shown in Table 4, specified in AISC 341-16 for the beam-to-column moment connections, was considered to obtain cyclic response of the all specimens. This loading was applied to the tip of the beam as the displacement controlled load. In order to simulate the cyclic loading, dynamic implicit procedure was used with the quasi-static application in ABAQUS.

Two analyses steps were considered for the connection models with fully restrained bolted beam splice, while one step was considered for the connection models without beam splice. For the connections with bolted beam splice, after the first step in which the pretension loads was applied, the loading history sequence in AISC 341-16 was introduced to the tip of the beam in the second step. Since there was no any bolted connection due to absence of beam splice, the loading sequence specified in AISC 341-16 was directly applied in the first step.

3.2 Response indices

Since the crack initiation was not explicitly modeled in this study, rupture index (RI) was defined in order to evaluate the connection configurations for ductile fracture potential (Kim *et al*. 2016 and Ricles *et al*. 2003). For this, RI is obtained at the specified locations expected to be experienced large plastic deformation during cyclic loading. RI is defined as shown in Eq. (2).

$$RI = \frac{\varepsilon_p / \varepsilon_y}{\exp(-1.5\dfrac{\sigma_m}{\sigma_{eff}})} \tag{2}$$

In Eq. (2), ε_p, ε_y, σ_m and σ_{eff} are the equivalent plastic strain, yield strain, hydrostatic stress and von Mises stress (equivalent stress) respectively.

Local plastic strain demand is measured by PEEQ defined as the ratio of plastic equivalent strain to yield strain (Ricles *et al*. 2003). PEEQ is defined as shown in Eq. (3).

$$PEEQ = \frac{\sqrt{\dfrac{2}{3}\varepsilon_{ij}^{p}\varepsilon_{ij}^{p}}}{\varepsilon_y} \tag{3}$$

In Eq. (3), ε_{ij}^{p} represent the plastic strain components.

3.3 Verification of finite element models

In order to verify the method to be adopted in this study for the models with the connection having fully restrained beam splice, the cyclic test results obtained from the experiment, containing a specimen with similar connection (CT), conducted by Oh *et al*. (2014) was considered; whereas for the connection model without beam splice, the cyclic test results obtained from the experiment, containing a specimen with a pre-qualified welded unreinforced flange-welded web connection (WUF-W), carried out by Han *et al*. (2015) was used.

The connection models based on the information obtained from the related researches on the experimental details were analyzed using the ABAQUS finite element program. Hysteresis loops, as a function of flexural moment resistance at column face and story drift angle, were obtained. As the hysteresis loops obtained from the analysis and the experiments were compared, since the results from

Table 4 AISC 341-16 loading sequence

Story drift angle*	0.00375	0.005	0.0075	0.01	0.015	0.02	0.03	0.04
Number of cycles	6	6	6	4	2	2	2	2

* Continue loading at increments of $\theta = 0.01$ rad, with two cycles at each loading step

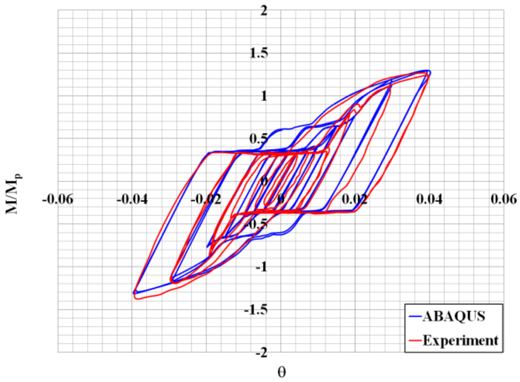

(a) Specimen CT

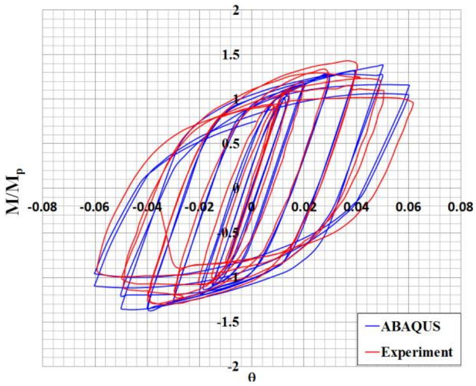

(b) Specimen WUF-W

Fig. 3 Comparison of the hysteresis loops

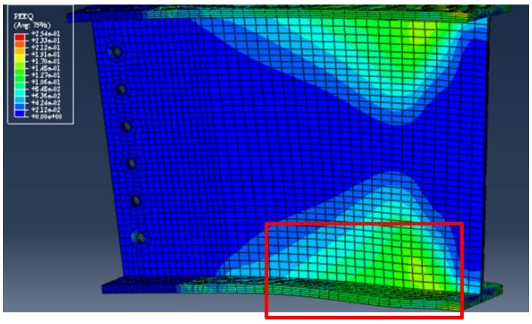

(a) Failure mode obtained from FEM

(b) Failure mode obtained from test

Fig. 4 Comparison of the failure modes of CT

the finite element analysis were in good agreement with the experiments, the definitions used in ABAQUS were decided to be applicable for the simulation of the connection models under cyclic loading, as shown in Figs. 3(a)-(b).

When the moment-rotation curve from the model of the Specimen CT shown in Fig. 3(a) is compared with that from the test, a good agreement which verifies the modeling technique has been observed, except of the bulges developed on the curves from the FEM. The formation of the bulges can be explained as follows: The plateau up to beginning of the bulge shows uniform slip occurred on both side of the connection, which causes contact between the bolt bodies and hole edges on the side of the beam segment with increasing rotation. After this point, the curve gains rigidity until a small slip occurs between the faying surfaces on the side of cantilever beam. Following this slip, once a contact between bolts and hole edges takes place, an increase in stiffness of the connection has been observed. It should be noted that this behavior similar to that from the test results obtained by Oh *et al*. (2016) observed in the model, is caused by the bolt installation performed in such a way that the same tolerance is uniformly provided between the bolts and hole edges, which is almost impossible to be able to put this into practice.

The failure mode of the both specimens was the local buckling of the beam flanges which lead to a reduction in strength. The local buckling mode of the beam flange obtained from the test and the FEM was shown in Figs. 4(a)-(b) for the connection with fully restrained bolted beam splice. It can be shown that the result from the test and the FEM were in good agreement.

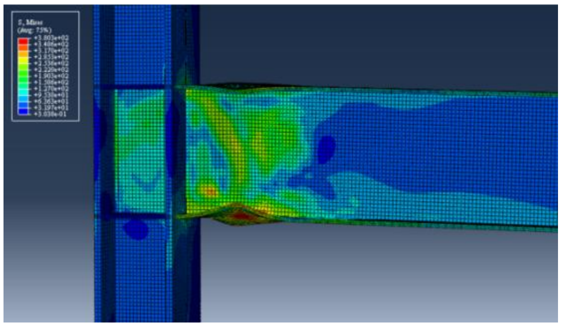

Fig. 5 Failure mode of the FEM of WUF-W connection

Since there was not any picture related to the failure mode from the experiment for another model, welded unreinforced flange-welded web connection, Fig. 5 shows only the post-buckling deformation localized in the flanges, which is mostly observed as a failure mode in this type of connections, obtained from the finite element analysis.

4. Finite element analysis results

As mentioned before, the loading history specified in

AISC 341-16 was applied and all analyses were performed under displacement control conditions. The behavior of the connection models was observed and summarized during the cyclic loading.

4.1 Finite element analysis observations

For the specimen CIP, yielding of beam flange and yielding around the bolt holes nearest to the column face was initiated during the cycles of 0.5% story drift. From the cycles of the 0.5% to the 3%, it was observed that the plastic deformations increased and expanded from the flange to the web, whereas they were limited around the bolt holes closest to the column face. During the cycles of 6% story drift, it was seen that plastic deformations increased more, and they were dramatically concentrated around the closest bolt holes to the column face, as shown in Fig. 6.

Since it was designed as the slip critical connection, the bolt slip was not occurred during the analysis.

For the specimens of COP and CWB exhibited quite similar behavior under cyclic loading. First, the plastic deformations occurred with the yielding of the beam during the cycles of 1% story drift. Then, it was observed that the plastic deformation increased and expanded from the flange to the web through the story drift of the 1% to the 6%, as shown in Fig. 7. At the end of the cycles for the story drift of 6%, local buckling initiation at the beam compression flange of the two specimens was observed. The only notable difference between the specimens was that in the specimen of COP, at the 1% story drift, the yielding around the bolt holes closest the column face was started.

4.2 Hysteresis loops

The hysteresis loops as a function of beam end-point normalized flexural moment (M/M_p) at the column face and the story drift ratio were obtained by applying a displacement controlled cyclic loading defined in AISC 341-16, to the beam end. Normalized flexural moment was obtained in such a way that the plastic moment of the beam (M_p) was divided by the beam end-point flexural moment at the column face (M) obtained from every steps of the finite element analysis.

According to the obtained hysteresis loops, all connection models satisfied the requirement for the special moment frame connections providing at least $0.80M_p$ of flexural moment resistance, determined at column face, at a story drift angle of 0.04 rad, as stated in AISC 341-16.

As seen from Fig. 8(a), the specimen CIP exhibited excellent performance based on the stable hysteresis loops of under cyclic loading, achieving the maximum flexural moment resistance at the story drift angle of 0.04 rad as specified in AISC 341-16, although the beam splice had been located in the protected zone. The specimen COP and CWB also exhibited quite sufficient performance and reached the same level of the flexural strength at the story drift angle of 0.04 rad.

While the normalized flexural strength of the specimens of COP and CWB obtained from the analysis results at the story drift of 0.04 rad were 1.25, it was obtained as 1.42 for the specimen CIP.

In the scope of this study, the effects of the slippage of the bolts in plastic hinge zone that would occur if the friction force on between splice plates is exceeded due to

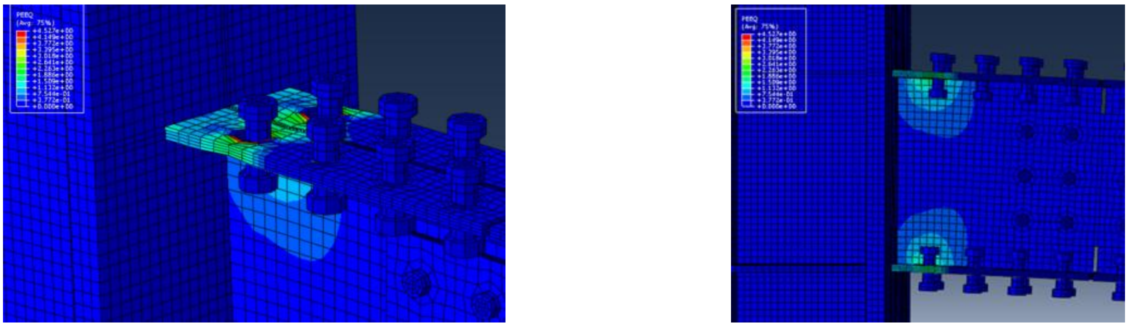

Fig. 6 Plastic deformations of CIP at 6% story drift

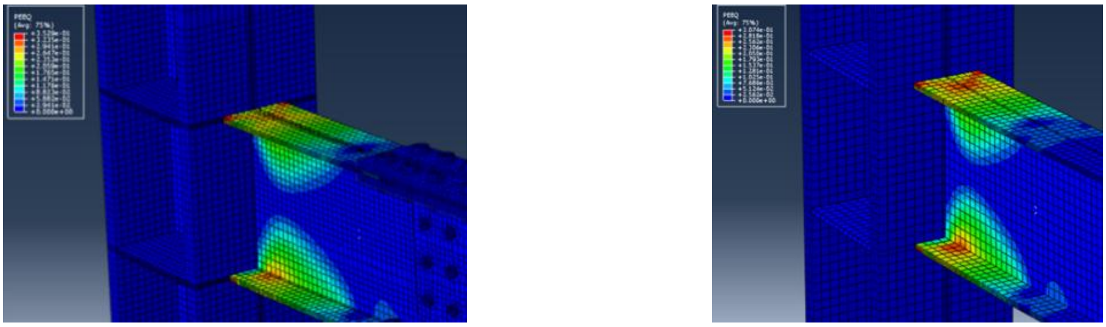

(a) COP at 6% story drift (b) CWB at 6% story drift

Fig. 7 Plastic deformations at 6% story drift

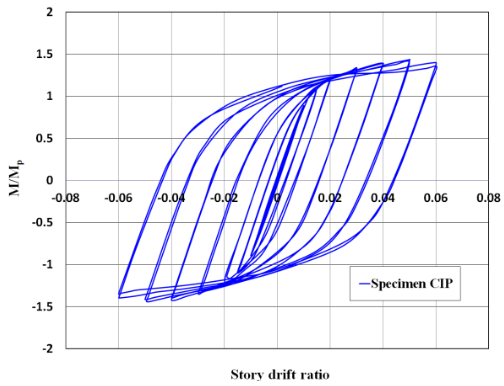

(a) Specimen CIP

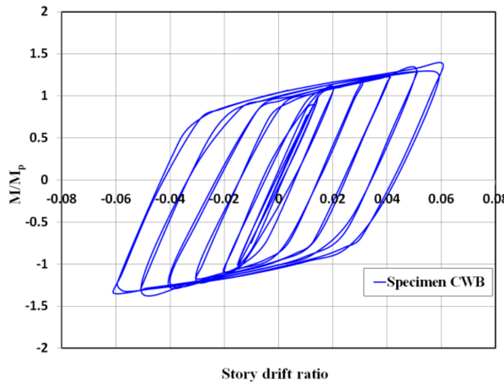

(b) Specimen CWP

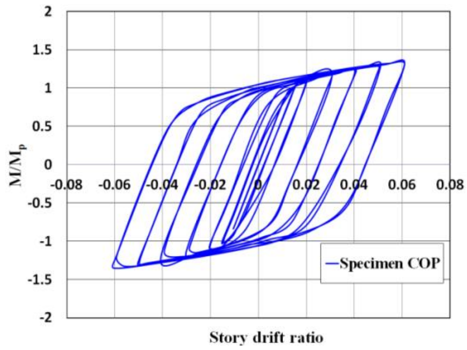

(c) Specimen COP

Fig. 8 Hysteresis loops of the connection models

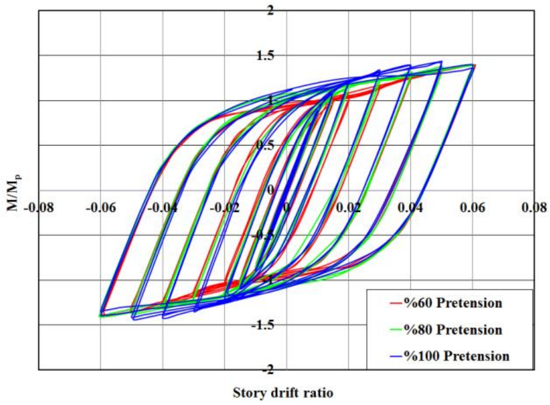

Fig. 9 Effect of pretension loss on specimen CIP

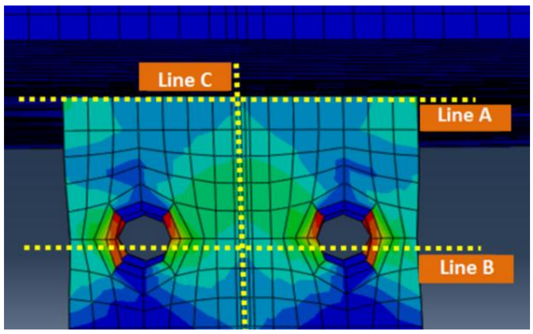

Fig. 10 Lines in which the PEEQ and RI calculated

a possible loss of pretension in the bolts were also investigated. Accordingly, the specimen CIP was modeled and analyzed considering that the pretension forces for the types of 10.9 M20 and M27 bolts were reduced by the ratio of 20% and 40%.

As seen in Fig. 9, the hysteresis loops show that due to the pretension loss in the bolts, the friction force on the contact surfaces were exceeded, resulting in a relative slippage; however, the reduction in the energy dissipation capacity of the connection was observed to be insignificant.

4.3 Analytical evaluation of the fracture potential (PEEQ and RI)

Since the fracture formation is not defined in the stress-strain behavior of the material in the connection models, analyses results were evaluated by using the RI and PEEQ for the regions with high local plastic strain demand in which the fracture initiation could occur.

PEEQ and RI indices were calculated along three lines at the rotation of 0.04 to determine the stress distribution and plastic strain demand in the locations where the plastic deformations quietly concentrated, as shown in Fig. 10.

Along the line A, it was observed that plastic deformation demand in specimen CIP was greater than the other models (Fig. 11). In addition to this, it was also shown that the plastic demand around the edges of the beam flange was obtained greater than that being at the middle portion of the line A.

The effect of the loss in cross-section area in the protected zone due to the bolt holes in the beam flange could be seen in Fig. 12, since the line B passed through the

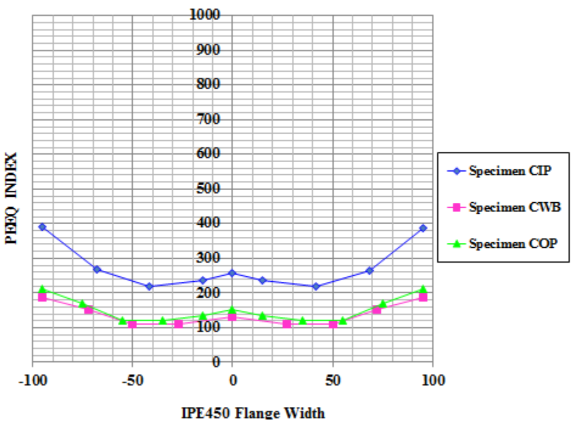

(a) PEEQ

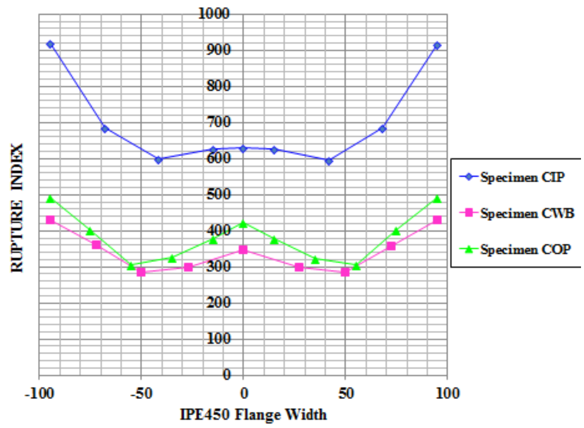

(b) RI

Fig. 11 PEEQ and RI along the line A

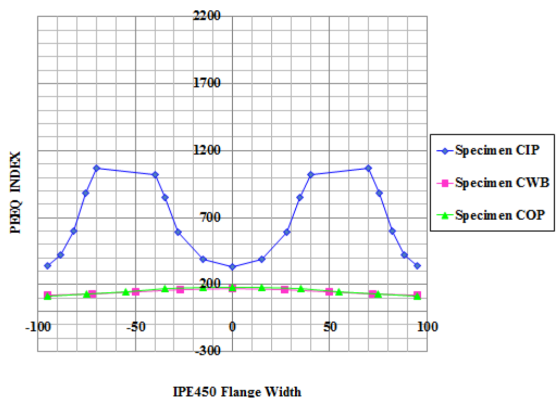

(a) PEEQ

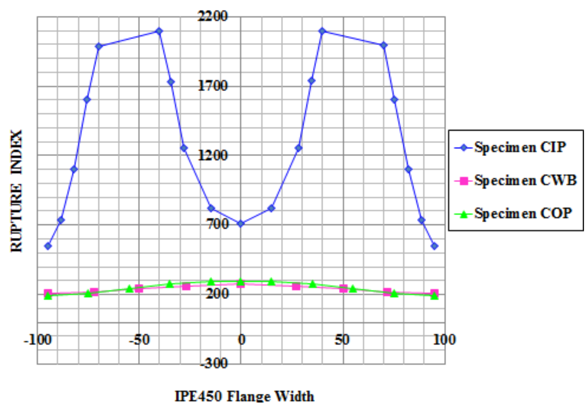

(b) RI

Fig. 12 PEEQ and RI along the line B

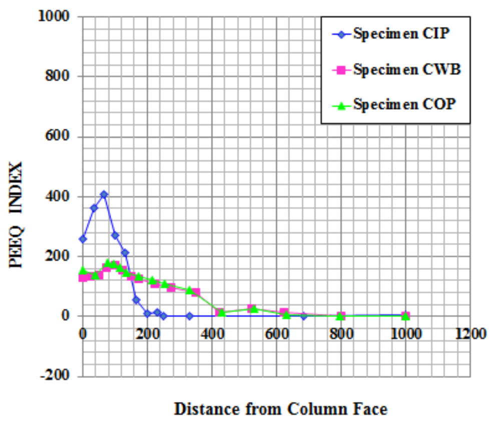

(a) PEEQ

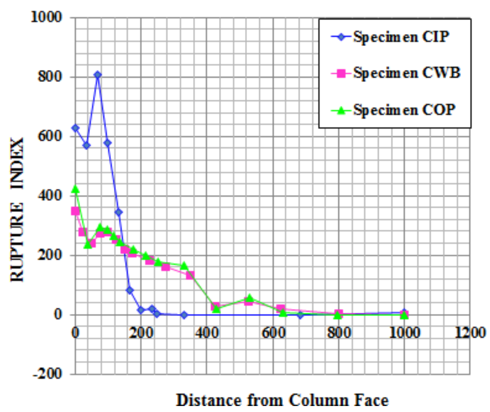

(b) RI

Fig. 13 PEEQ and RI along the line C

bolt holes closest to the column face. In specimen CIP, the RI index was about 2000 around the bolt holes, whereas it was around 710 in the middle of the line B, corresponding about 36% of which obtained around the holes. This increase indicated that the probability of crack formation around the holes was higher than the middle portion of the beam flange. As there was no discontinuity or loss of cross-section in the plastic hinge region, it could be indicated that there was no circumstance that would cause local crack formation in the other connection models.

As can be seen in Fig. 13, along the line C, PEEQ and RI calculated for the specimen CIP showed sudden changes in a limited area, where the bolt holes closest to the column face was located, while these indices show a more regular

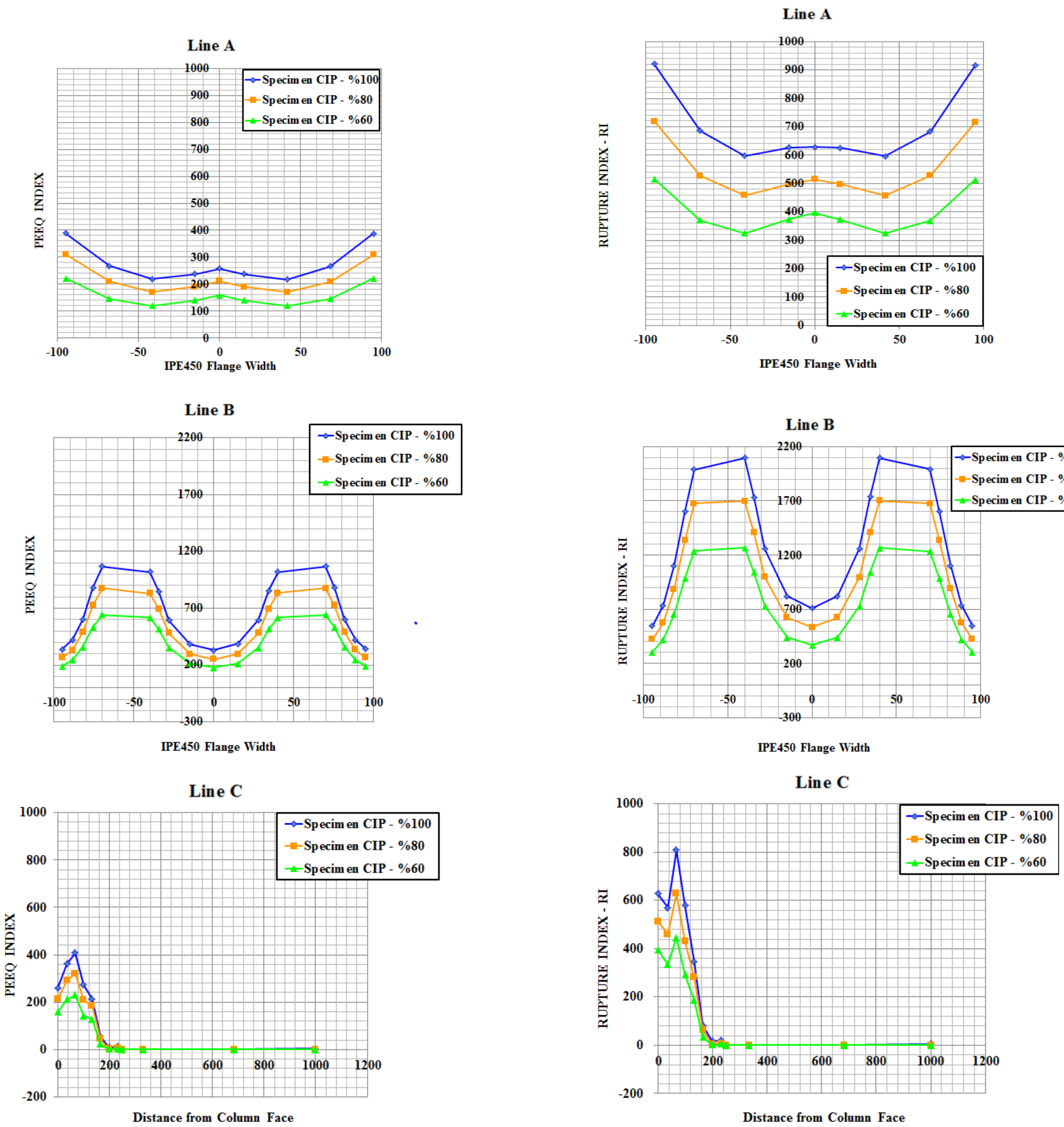

Fig. 14 Effect of pretension loss on PEEQ and RI

change in a wider area in the other specimens. This also shows that all plastic deformations accumulate in the region bounded by the reduced cross-sectional area.

As seen in Figs. 11, 12 and 13, in the specimen CIP, compared to the other specimens, RI was found to be higher due to the formation of the stress-strain concentration around the bolt holes closest to the column face in the beam flange. Therefore, it was decided that the probability of fracture formation was higher in these regions and also it has to be investigated experimentally.

For the specimen CIP, PEEQ and RI were also calculated along the line A, B, and C for the FEMs with 60% and 80% pretension loads applied in order to determine how the loss of the pretension in the bolts affect the plastic deformation demand and the crack initiation potential.

As seen in Fig. 14, it was obtained that the plastic deformation demand decreased with the increase in loss of pretension. This was because that the relative slippage between the surfaces of the splice plates was occurred, the amount of the rotation at the splice increased with the effect of the pretension loss. Thus, due to the decrease on the demand of the bending moment and the plastic deformation, the PEEQ and RI were obtained smaller in the models having loss of pretension than that obtained by applying full pretension.

5. Conclusions

In the scope of this study it was investigated that how a fully restrained bolted beam splice joint used for a column-tree connection affects the beam-to-column connection behavior in the steel special moment frames under cyclic loading when located within the plastic hinge zone. The recommendations and key results are summarized as follows:

- The specimen CIP having a fully restrained bolted beam splice within the plastic hinge zone had a discontinuity in the beam flange due to the bolt holes leading to the cross-section loss in this zone. However, when the hysteresis loops obtained from the numerical analysis under cyclic loading are examined, it is seen that the specimen CIP exhibited excellent cyclic performance exceeding the maximum flexural moment resistance of $0.80M_p$ at column face at the story drift angle of 0.04 rad, as stated in AISC 341-16.
- The specimens COP and CWB also were satisfied the requirement as stated in AISC 341-16 since the measured flexural moment resistance at column face is found to be higher than $0.8M_p$ at 0.04 rad.
- In the specimen CIP the plastic deformations were concentrated in limited area between the column face and the bolt holes closest to the column face, whereas in specimens of COP and CWB, they spread over the wide region on the beam.
- RI was defined in order to evaluate the connection configurations for ductile fracture potential, since the crack initiation was not explicitly modeled in this study. As defined earlier on the line B around the bolt holes closest to column face, RI was obtained about 1800 for specimen CIP, whereas it was obtained about 200 for the other specimens. For this reason, it is seen that the probability of crack formation around the bolt holes is found to be high. This case, therefore, indicates that the effect of high concentration of plastic deformation around the bolt holes has to be also experimentally investigated.
- In specimen CIP, the loss of the pretension in the bolts caused the formation of the relative slip between the contact surfaces. Although the formation of slippage reduced the energy dissipation capacity, it could be said that sufficient flexural resistance was achieved at the story drift of 4%, and it did not have significant negative impact on the connection behavior. However, it should be noted that lateral deformation of the whole structure will be increased due to rotation in the column-tree connection induced by the slippage.
- According to analysis results, it is observed that any loss of pretension in the bolts causes to significantly decrease the crack initiation potential depending on the reduction in the RI and PEEQ at the critical sections.

References

ABAQUS (2017), Analysis User's Guide, Hibbit, Karlsson, and Sorenson, Inc., Pawtucket, RI, USA.

ABAQUS (2017), Getting Started with ABAQUS: Interactive Edition, Hibbit, Karlsson, and Sorenson, Inc., Pawtucket, RI, USA.

AISC (2016), ANSI/AISC 341-16, Seismic provisions for structural steel buildings, American Institute of Steel Construction Inc., Chicago, IL, USA.

AISC (2016), ANSI/AISC 358-16, Prequalified connections for special and intermediate steel moment frames for seismic applications, American Institute of Steel Construction Inc., Chicago, IL, USA.

AISC (2016), ANSI/AISC 360-16, Specification for structural steel buildings, American Institute of Steel Construction Inc., Chicago, IL, USA.

Astaneh, A. (1997), "Seismic design of steel column-tree moment-resisting frames", Structural Steel Educational Council Technical Information & Product Service, University of California, Berkeley, CA, USA.

Han, S.W., Kwon, G.U. and Moon, K.H. (2007), "Cyclic behavior of post-Northridge WUF-B connections", *J. Constr. Steel Res.*, **63**, 365-374.

Han, S.W., Moon, K.H., Hwang, S.H. and Stojadinovic, B. (2015), "Seismic performance evaluation of intermediate moment frames with reduced beam section and bolted web connections", *Earthq. Spectra*, **31**(2), 895-919.

Han, S.W., Kim, N.H. and Cho, S.W. (2016), "Prediction of cyclic behavior of WUF-W connections with various weld access hole configurations using nonlinear FEA", *Int. J. Steel Struct.*, **16**(4), 1197-1120.

Kaufmann, E.J., Metrovich, B. and Pense, A.W. (2001), "Characterization of Cyclic Inelastic Strain Behavior on Properties of A572 Gr. 50 and A913 Gr. 50 Rolled Sections (ATLSS Report No. 01-13)", Lehigh University, Bethlehem, PA, USA.

Kim, D.W., Ball, S.C., Sim, H.B. and Uang, C.M. (2016), "Evaluation of sloped RBS moment connections", *J. Struct. Eng., ASCE*, **142**(6), 04016013.

Kumar, P.C.A., Sahoo, D.R. and Kumar, N. (2015), "Limiting values of slenderness ratio for circular braces of concentrically braced frames", *J. Constr. Steel Res.*, **115**, 223-235.

Lee, K., Li, R., Chen, L., Oh, K. and Kim, K.S. (2014a), "Cyclic testing of steel column-tree moment connections with various beam splice lengths", *Steel Compos. Struct., Int. J.*, **16**(2), 221-231.

Lee, K., Yang, Y., Chen, L., Oh, K. and Hong, S.B. (2014b), "Behavior and design recommendations of splice connection in weak-axis column-tree steel moment frames", *Adv. Mater. Res.*, **1025-1026**, 902-905

Lee, K., Oh, K. and So, J. (2016), "Bolt slippage evaluation in column-tree steel moment connection on L/d", *Proceedings of the World Congress on Civil, Structural, and Environmental Engineering* (*CSEE'16*), Paper No. ICSENM 114, Prague, Czech Republic.

Oh, K., Li, R., Chen, L., Hong, S.B. and Lee, K. (2014), "Cyclic testing of steel column-tree moment connections with weakened beam splices", *Int. J. Steel Struct.*, **14**(3), 471-478.

Oh, K., Lee, K., Chen, L., Hong, S.B. and Yang, Y. (2015), "Seismic performance evaluation of weak axis column-tree moment connections with reduced beam section", *J. Constr. Steel Res.*, **105**, 28-38.

Oh, K., So, J., Ha, H. and Lee, K. (2016), "Seismic performance evaluation of Korean column-tree steel moment connections", *Int. J. Steel Struct.*, **16**(4), 1287-1298.

Okazaki, T., Engelhardt, M.D., Drolias, A., Schell, E., Hong, J.K. and Uang, C.M. (2009), "Experimental investigation of link-to-column connections in eccentrically braced frames", *J. Constr. Steel Res.*, **65**(7), 1401-1412.

Ricles, J.M., Mao, C., Lu, L.W. and Fisher, J.W. (2003), "Ductile details for welded unreinforced moment connections subject to

inelastic cyclic loading", *Eng*. *Struct*., **25**, 667-680.
Turkish Code for Design and Construction of Steel Structures (2016), T. RT. Official Journal, 29614, February 4th 2016, Turkey.
Vasdravellis, G., Uy, B., Tan, E.L. and Kirkland, B. (2012), "Behaviour and design of composite beams subjected to negative bending and compression", *J*. *Constr*. *Steel Res*., **79**, 34-47.

CC